GMR
The Original

FABRICATION OF BIOCOMPATIBLE POLYMERIC ELECTROSPUN NANOSCAFFOLDS EMBEDDED WITH CUO NANOPARTICLES FROM BROWN MARINE MACROALGAE EXTRACT FOR ENHANCED WOUND HEALING ACTIVITY ON HACAT CELLS

Srinidhi Rajaraman[1], Thayasre Babu[2], Santhosh Kumar Thangamani[3], David Jayaseelan Baranabas[4], Narasimhalu CRV[5*]

[1]Saveetha Medical College & Hospital (SMCH), Saveetha Institute of Medical and Technical Sciences (SIMATS), Thandalam, Chennai, Tamil Nadu 602105, India. srinidhirajaraman04@gmail.com
[2]Department of Dermatology, Saveetha Medical College and Hospital, Saveetha Institute of Medical And Technical Sciences (SIMATS), Thandalam, Chennai-602105, Tamil Nadu, India. 141.thayasrebabu@gmail.com; https://orcid.org/0009-0001-7522-5357
[3]Department of Pediatrics, Saveetha Medical College and Hospital, Saveetha Institute of Medical and Technical Sciences (SIMATS), Thandalam, Chennai-602105, Tamil Nadu, India. santhoshdnbmbbs@gmail.com
[4]Department of Microbiology, Nehru Arts and Science College, Coimbatore-641105, Tamil Nadu, India. nascdavidjayaseelan@nehrucolleges.com; https://orcid.org/0000-0002-2619-8524
[5*]Department of Dermatology, Saveetha Medical College and Hospital, Saveetha Institute of Medical And Technical Sciences (SIMATS), Thandalam, Chennai-602105, Tamil Nadu, India. drnarasimhalu@yahoo.co.in; https://orcid.org/0009-0005-8261-5512

ABSTRACT

This study investigated the synthesis, characterization, and wound healing potential of brown seaweed extract, green-synthesized copper oxide nanoparticles (CuO NPs), and starch/polyvinyl alcohol (PVA)/CuO-NPs nanoscaffolds. UV-Visible spectroscopy confirmed the presence of UV-sensitive metabolites in the algal extract (peak at 267 nm) and revealed a surface plasmon resonance (SPR) band for CuO NPs at 292 nm, indicating nanoparticle formation. Fourier-transform infrared spectroscopy (FTIR) analysis identified functional groups involved in CuO NP stabilization and scaffold interactions, while X-ray diffraction (XRD)confirmed the monoclinic crystalline structure of CuO NPs and their successful incorporation into the semi-crystalline starch/PVA matrix. Scanning electron microscopy (SEM) images showed uniform CuO NP distribution within porous nanofibers, ideal for tissue regeneration. Thermogravimetric analysis (TGA) demonstrated enhanced thermal stability in CuO-loaded scaffolds. Dynamic light scattering (DLS) revealed moderate colloidal stability (zeta potential: –10.03 mV) with a hydrodynamic diameter of 125.6 nm. In the wound healing assay, all samples exhibited concentration-dependent activity. The algal extract achieved 74% closure at 100 µg/mL, while CuO NPs showed superior efficacy (88%). However, the starch/PVA/CuO-NPs nanoscaffold demonstrated the highest wound closure (100%), attributed to its structural support and bioactive CuO NP release. These findings highlight the scaffold's potential as an advanced wound dressing, combining biocompatibility, thermal stability, and enhanced regenerative properties for accelerated tissue repair.

KEYWORDS: *Pocockiella variegata*; Green synthesis; Starch/PVA/CuO-NPs nanoscaffolds; Wound healing

1. INTRODUCTION

Wound healing is a multifaceted and dynamic biological process involving coordinated interactions among cells, extracellular matrix components, and various signaling molecules to restore the integrity of injured skin [1]. Despite advances in wound care, challenges such as prolonged healing time, infections, and poor tissue regeneration remain significant clinical concerns [2]. These issues are particularly pronounced in patients with chronic wounds, diabetic ulcers, and pressure sores [3]. Conventional wound dressings such as gauze and cotton pads often lack functionalities such as antibacterial properties, controlled moisture retention, or the ability to stimulate tissue regeneration [4]. Therefore, the development of novel wound dressings with bioactive, biodegradable, and biocompatible properties has become a key research priority in regenerative medicine and tissue engineering [5].

Nanotechnology offers promising solutions in this field by enabling the design of advanced wound healing platforms that not only protect the wound site but also actively promote healing through controlled drug delivery and interaction with cellular processes [6]. In particular, nanofibrous scaffolds produced through electrospinning techniques have garnered substantial interest due to their structural similarity to the extracellular matrix, high surface area-to-volume ratio, and porosity, which support cell adhesion, proliferation, and nutrient transport [7]. Among various natural and synthetic polymers used for electrospinning, starch and polyvinyl alcohol (PVA) stand out due to their favorable physicochemical and biological properties [8].

Starch, a naturally abundant polysaccharide, is widely recognized for its biodegradability, renewability, and biocompatibility [9]. However, its inherent brittleness and water sensitivity can limit its standalone application in scaffold fabrication [10]. Blending starch with PVA—a synthetic, water-soluble, and non-toxic polymer—improves its mechanical

strength, thermal stability, and electrospinnability, making the composite suitable for biomedical applications [8]. The starch/PVA blend forms a stable nanofibrous matrix capable of encapsulating bioactive agents, thereby enabling the development of functional scaffolds with enhanced therapeutic effects [11].

Incorporating metal oxide nanoparticles into polymeric nanofibers has further expanded the utility of these scaffolds by providing additional properties such as antibacterial activity, oxidative stress modulation, and enhanced tissue regeneration [12]. Among metal oxide nanomaterials, copper oxide nanoparticles (CuO NPs) have shown exceptional promise due to their potent antimicrobial activity, pro-angiogenic properties, and ability to promote collagen deposition [13]. However, conventional physical and chemical synthesis methods for CuO NPs often involve hazardous reagents, high energy inputs, and generate environmentally harmful byproducts [14].

To overcome these limitations, green synthesis approaches utilizing plant and marine-derived extracts have emerged as eco-friendly alternatives for nanoparticle production [15]. These biological systems are rich in reducing and stabilizing agents such as polyphenols, flavonoids, proteins, and polysaccharides, which not only facilitate nanoparticle formation but also enhance their biological activity [16]. Marine macroalgae, in particular, have gained attention as sustainable bioresources due to their abundance, rapid growth, and diverse biochemical composition [17].

Pocockiella variegata, a brown seaweed native to coastal regions such as Rameswaram in Tamil Nadu, India, is rich in bioactive compounds with antioxidant, antimicrobial, and anti-inflammatory potential [18]. Despite its therapeutic promise, its application in nanobiotechnology remains underexplored. Leveraging its bioactives for the green synthesis of CuO NPs can offer a dual benefit: synthesizing functional nanomaterials and enhancing their wound healing efficacy [19]. Furthermore, the use of ultrasound-assisted extraction techniques enables the efficient recovery of thermolabile and water-soluble compounds from the algal biomass, improving extract yield and activity [20].

In the current study, reports the fabrication of a novel electrospun nanoscaffold composed of a starch/PVA polymer matrix embedded with green-synthesized CuO NPs derived from Pocockiella variegata extract [21]. The CuO NPs were synthesized using an ultrasonic-assisted green synthesis method, which enhances reaction kinetics and nanoparticle uniformity [22]. The nanoscaffolds were systematically characterized for their optical, structural, thermal, morphological, and surface properties using UV–Visible spectroscopy, Fourier-transform infrared spectroscopy (FTIR), X-ray diffraction (XRD), scanning electron microscopy (SEM), dynamic light scattering (DLS), and thermogravimetric analysis (TGA) [23].

Biological evaluation of the wound healing potential was carried out using an in vitro scratch assay on human keratinocyte (HaCaT) cells [24]. The assay enabled the assessment of cell migration and wound closure capability in response to treatment with the algal extract, CuO nanoparticles, and the CuO-loaded nanoscaffold [25]. The study revealed that while the algal extract and CuO NPs demonstrated significant wound closure, the starch/PVA/CuO nanoscaffold exhibited the highest healing efficacy, indicating a synergistic effect of the polymer matrix and bioactive nanoparticles in promoting tissue regeneration.

This research contributes to the growing field of marine algal biotechnology and green nanotechnology by presenting an integrative approach to wound healing. The use of an eco-friendly synthesis route, combined with a biodegradable polymer system, underscores the potential of this scaffold as a next-generation wound dressing material [26]. Importantly, the findings pave the way for the clinical translation of biocompatible nanoscaffolds that align with principles of sustainability, safety, and therapeutic efficacy [27].

2. MATERIALS AND METHODS

2.1. Materials

Pocockiella variegata, a marine alga, was sourced from the coastal region of Rameswaram in Tamil Nadu, India, for this investigation. Copper (II) sulfate pentahydrate ($CuSO_4 \cdot 5H_2O$), obtained from Sigma-Aldrich, served as the precursor salt for synthesizing CuO NPs. PVA (MW 115,000) was utilized as the primary polymer matrix for electrospinning, and locally available starch was blended into the nanofiber matrix. Analytical-grade chemicals and solvents such as Milli-Q water and ethanol were procured from Merck and Sigma-Aldrich. Electrospinning was conducted using a HOLMARC HO-NFES-040 high-voltage setup with a syringe pump to fabricate PVA/CuO NP nanofibers. Material characterization was performed using a VIS SPEC V-730 UV–Vis spectrophotometer, a Spectrum Two (PerkinElmer) FTIR spectrometer, a Bruker D8 Advance XRD instrument, and a JSM-IT800 NANO SEM. Additional analyses, including particle size and zeta potential measurements, were carried out using a Malvern Zetasizer Ultra. Thermal analysis was done with a PerkinElmer TGA 8000. HaCaT keratinocyte cells were obtained from the National Centre for Cell Science (NCCS), Pune, India, which provided authenticated and contamination-free cell stocks for biological investigations focused on wound healing efficacy.

2.2. Collection of marine macroalgae

Samples of *Pocockiella variegata* were collected from the intertidal zones near Rameswaram, Tamil Nadu. The collected *Pocockiella variegata* was taxonomically identified and authenticated by Dr V. Veeragurunathan, CSIR-CSMCRI-Marine Algal Research Station, Mandapam Camp 623519, Tamil Nadu, India. A voucher specimen was prepared and deposited at the Herbarium of the CSIR-CSMCRI-Marine Algal Research Station, under the accession number: SI–2025–RMM–024. This authentication ensures botanical accuracy and standardization of the study material. Upon authentication, algae were initially washed with tap water to eliminate sand, debris, and other extraneous materials, followed by multiple rinses with distilled water. Around 100 grams of the cleaned algal biomass were chopped into small fragments and air-dried at room temperature over a period of 14 days. Once thoroughly dried, the material was ground into a fine powder using a mechanical grinder. The resulting powder was stored in a moisture-free, airtight container until further use in extraction and nanoparticle synthesis processes.

2.3. Ultrasonic extraction of algal bioactives

To extract the bioactive ingredients, 2 grams of the powdered *Pocockiella variegata* were combined with 50 mL of Milli-Q water in a sterile 100 mL beaker. This mixture was subjected to ultrasonic extraction using a LABQUEST ultrasonic bath (Borosil, Serial No. 941032329018) at 60°C for 45 minutes. After sonication, the suspension was filtered using sterile Whatman No. 1 filter paper to remove solid residues. The clear filtrate was collected in a sterile vessel and preserved at 10°C. For subsequent procedures, the aqueous extract was lyophilized using a freeze dryer to obtain the dry extract in powdered form for ease of incorporation in downstream applications [28, 29].

2.4. Eco-friendly synthesis of CuO NPs

The biosynthesis of CuO NPs was accomplished by mixing 50 mL of 0.1 M $CuSO_4 \cdot 5H_2O$ solution with 10 mL of aqueous algal extract prepared by dissolving 10 mg of freeze-dried extract in 10 mL of Milli-Q water, ensuring a 5:1 solution ratio. The blend was stirred magnetically at 650 rpm and maintained at 60°C for 2 hours. The change in color from blue to light bluish-green indicated the formation of nanoparticles. The resultant solution was rinsed three times with distilled water under identical heating and stirring conditions to eliminate any remaining impurities. The purified CuO NP suspension was freeze-dried for 48 hours to obtain the final powdered product [30].

2.5. Electrospinning of starch/PVA nanofibers embedded with CuO NPs

To prepare the nanofibers, a 15% (w/w) PVA solution was first made using distilled water. Into this, 100 mg of starch and 100 mg of biosynthesized CuO NPs were introduced. The solution was stirred vigorously at 50°C for 2.5 hours until a uniform mixture was obtained. This polymer composite was electrospun using the HOLMARC HO-NFES-040 electrospinning unit equipped with an HMPSKV30 power supply (0–30 kV, 0.5 mA). The solution was loaded into a syringe fitted with a needle of 0.84 mm internal diameter. Electrospinning was carried out at 11.5 kV, with a 12.3 cm gap between the needle and collector, and a flow rate of 0.4 mL/h. Nanofibers were collected over aluminum foil for 6 to 8 hours at ambient room conditions [31-33].

2.6. Physicochemical characterization

2.6.1. UV–visible spectroscopy

The optical features of the algal extract, CuO NPs, and the CuO-loaded starch/PVA nanofibers were examined using a VIS SPEC V-730 UV–Vis spectrophotometer. The absorbance spectrum was recorded in the 200–800 nm range, using deionized water as the reference blank [34].

2.6.2. FTIR spectroscopy analysis

Chemical bonding and functional group identification in the algal extract, synthesized CuO NPs, and the CuO NP-loaded fibers were analyzed using a PerkinElmer Spectrum Two FTIR spectrometer operating in ATR mode. Each sample underwent 64 scans within the 4000–400 cm^{-1} range at a resoluti on of 4 cm^{-1} [35].

2.6.3. XRD analysis

The crystalline structure of the CuO NPs and the nanofiber composites was examined via XRD using a Bruker D8 Advance diffractometer equipped with CuKα radiation (λ = 1.5406 Å), operated at 40 kV and 40 mA. Data were captured across a 2θ range of 5° to 90°, with a step interval of 0.029649°[36].

2.6.4. SEM imaging

Surface morphology and structural properties were assessed using a JSM-IT800 NANO SEM (JEOL, Japan). Prior to imaging, all specimens were coated with a thin layer of gold to improve conductivity and enhance image resolution[37].

2.6.5. TGA

Thermal characteristics were evaluated using the PerkinElmer TGA 8000 system. Approximately 5 mg of each sample was placed in aluminum crucibles and heated from room temperature to 550°C at a rate of 15°C/min under a nitrogen environment. Weight loss patterns were monitored to determine thermal stability [38].

2.6.6. Particle size and zeta potential

The Malvern Zetasizer Ultra was employed to evaluate nanoparticle size and surface charge using DLS and electrophoretic mobility measurements. These analyses provided data on hydrodynamic diameter and zeta potential, indicating colloidal behavior [39]. All raw data from these analyses are available at Mendeley Data (doi: 10.17632/6tddv74p8k.1).

2.7. Wound healing (scratch) assay

A scratch assay was performed to assess the wound healing capacity of HaCaT keratinocyte cells when exposed to algal extract, CuO NPs, and CuO-loaded starch/PVA nanoscaffolds. Cells were seeded in 12-well plates at a density of 2×10^5 cells/well using DMEM medium containing 10% fetal bovine serum (FBS) and 1% penicillin-streptomycin. Incubation was carried out at 37°C with 5% CO_2 until a full monolayer formed. A sterile 200 µL pipette tip was used to make a linear scratch to mimic a wound. Post-scratch, wells were rinsed with PBS to remove detached cells. Cells were then treated with test samples at 6.25, 12.5, 25, 50, and 100 µg/mL concentrations in serum-free DMEM. Control wells received no treatment. Images of wound areas were captured at 0, 24, and 48 hours using a phase-contrast inverted microscope. The percentage wound closure was quantified using ImageJ software to assess the healing effect [40].

2.8. Statistical evaluation

All datasets were subjected to statistical analysis using SPSS version 25.0 and GraphPad Prism version 9.0. Results are presented as mean ± standard deviation from three independent experiments. One-way ANOVA was applied for comparing group means, with post-hoc analysis conducted via Tukey's or Dunnett's tests where relevant. A p-value < 0.05 was considered statistically significant. Pearson's correlation was used to assess variable relationships. Data distribution normality was evaluated using the Shapiro–Wilk test, and log transformation was applied to non-normal data. All statistical interpretations were made under a 95% confidence interval [41].

RESULTS

3.1. UV–visible spectroscopy

The UV–Visible absorption spectrum of the macroalgal-derived extract (Figure 1) exhibited a prominent peak at 267 nm with a maximum absorbance of 0.4035, indicative of the presence of UV-sensitive secondary metabolites. These may include phenolic or aromatic constituents possessing extensive conjugated systems. The absorbance values extended from 0.3285 to 0.4035 within the 200–800 nm wavelength range. Notably, the visible region (400–700 nm) showed minimal absorption, implying a reduced chlorophyll concentration, potentially caused by degradation or purification steps during extraction. In contrast, the green-synthesized CuO NPs revealed a distinct surface plasmon resonance (SPR) band at 292 nm with a heightened absorbance of 0.70716. This observed blue shift from the standard CuO SPR region (570–600 nm) can be ascribed to the nanoparticle size reduction, oxidative effects on the surface, or stabilization facilitated by bioactive compounds during synthesis. The CuO NPs exhibited an absorbance range from 0.31409 to 0.70716, and the sharp post-peak decline suggested the formation of homogeneously sized nanoparticles with minimal aggregation tendencies [42].

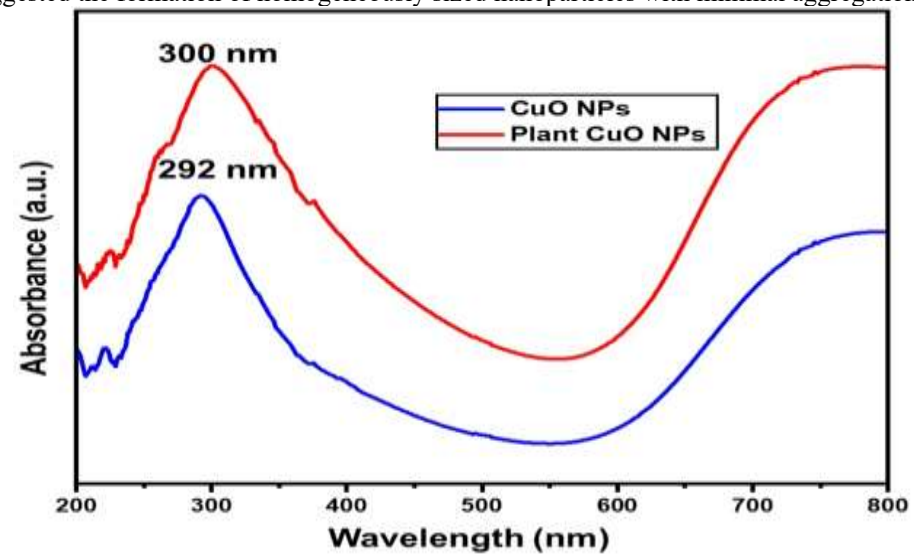

Figure 1: UV–Visible Spectroscopy analysis of algae extract and CuO NPs

3.2. FTIR spectroscopy analysis

FTIR spectroscopic analysis (Figure 2) provided insights into the functional groups involved in the synthesis and stabilization of the green-fabricated CuO NPs. A broad band centered at 3219.71 cm^{-1} signified stretching vibrations of hydroxyl (–OH) and amine (N–H) groups, most likely arising from phytochemicals that served as natural capping agents. Peaks located near 1509.94 cm^{-1} and within the 672–463 cm^{-1} zone were attributed to aromatic ring vibrations and Cu–O bonding, respectively, thereby confirming the successful formation of CuO NPs. For the starch/PVA scaffold, characteristic polymeric features were evident: an –OH stretch at 3295.71 cm^{-1}, C–H stretching around 2923.65 cm^{-1}, and ether bond (C–O–C) vibrations between 1141 and 1088 cm^{-1}. Notably, signals within 605–478 cm^{-1} indicated CuO NP presence embedded in the matrix. A shift in the hydroxyl absorption peak hinted at hydrogen bonding interactions between CuO NPs and the scaffold, which potentially improved the mechanical strength. Additionally, the appearance of a carbonyl stretch at 1711.09 cm^{-1} suggested oxidation of PVA or the interaction between CuO and PVA's carbonyl groups [43-47].

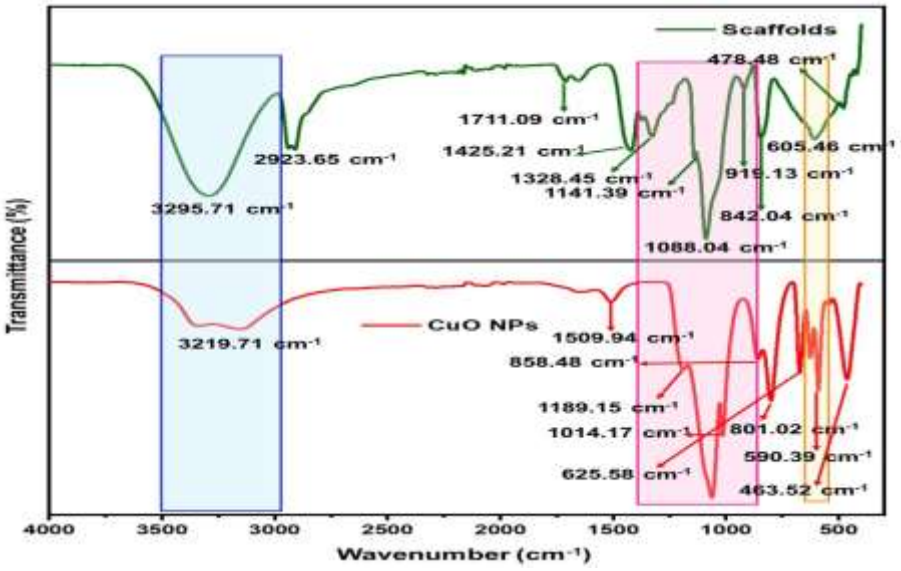

Figure 2: FTIR analysis of CuO NPs and nanoscaffolds

3.3. XRD analysis

XRD patterns (Figure 3) of the biosynthesized CuO NPs and CuO-integrated starch/PVA scaffolds revealed their crystalline nature. The CuO NPs exhibited sharp diffraction peaks at 2θ angles of 32.75°, 35.70°, 38.05°, 48.66°, 57.94°, 61.33°, and 75.48°, with interplanar spacings ranging from 1.59 to 3.67 Å. These reflections corresponded to monoclinic

CuO (JCPDS 48-1548), with no indications of Cu_2O impurities. The most intense peak at 35.70°, indexed to (002)/(111), showed a peak area of 141.86 Cps × °. Crystallite sizes were estimated to be between 20 and 50 nm using the Debye–Scherrer equation, with full width at half maximum (FWHM) values ranging from 0.1° to 0.9°. The CuO-loaded starch/PVA scaffold exhibited broader peaks at 21.35°, 22.97°, and 43.14° (2θ), indicating its semi-crystalline structure. Attenuated CuO peaks, particularly at 35.70°, 57.28°, and 61.33°, suggested nanoparticle encapsulation. The presence of a broad amorphous hump between 10° and 30°, along with lower FWHM values (0.16°–1.06°), indicated improved nanoparticle dispersion within the polymeric network. A negative peak at 39.46° was likely a result of instrumental artifacts. Overall, the data confirmed successful CuO synthesis and effective incorporation into the scaffold matrix, enhancing its potential for biomedical applications [48-51].

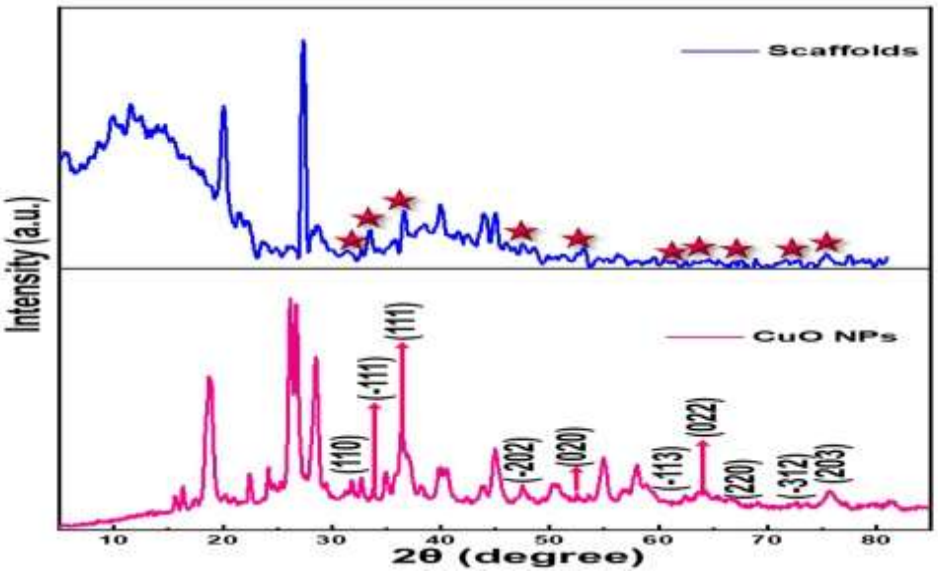

Figure 3: XRD analysis of CuO NPs and nanoscaffolds

3.4. SEM analysis

SEM images (Figure 4), captured using a gold-coated JSM-IT800 NANO SEM, illustrated the morphological features of the biosynthesized CuO NPs. The particles exhibited a mixture of spherical and irregular geometries, with diameters ranging from 50 to 200 nm. Clusters between 500 and 1000 nm were occasionally observed, which may result from partial nanoparticle agglomeration caused by electrostatic interactions. The particle surfaces appeared coarse, potentially due to phytochemical residues from the algal extract coating the particles. The electrospun starch/PVA nanofiber scaffolds embedded with CuO NPs displayed a continuous fibrous architecture free from bead formation. The fibers exhibited diameters between 150 and 300 nm and maintained a high degree of porosity. This porous structure is particularly advantageous for applications like wound healing and tissue regeneration. Bright, sub-200 nm particulates were uniformly distributed along the fiber length, confirming the even dispersion and integration of CuO NPs into the fibrous matrix, which preserved both the mechanical strength and morphological consistency of the scaffold [52].

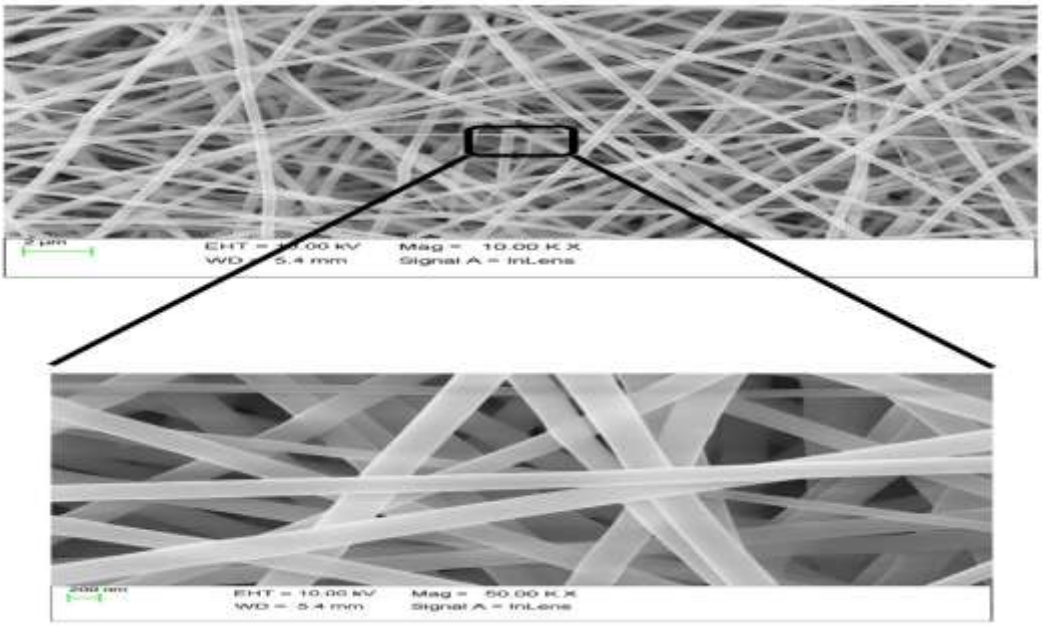

Figure 4: SEM analysis of starch/PVA/CuO-NPs nanoscaffolds

3.5. TGA

TGA under nitrogen conditions (Figure 5) assessed the thermal behavior of CuO-loaded starch/PVA scaffolds. The analysis revealed a total weight loss of 35.87%, while the residual mass was 64.13%, primarily comprising CuO and other

thermally inert materials. The degradation process occurred in three distinct phases. The initial phase (50–90°C) was associated with moisture evaporation and showed a peak degradation rate of –2.54%/min at 53.71°C. The main degradation stage commenced at 262.78°C and culminated at 326.36°C, which involved the thermal breakdown of the polymer backbone, especially C–C and C–O linkages, with a peak rate of –2.93%/min. The final degradation phase ended at 363.12°C and was linked to the decomposition of residual carbonaceous material. By comparison, native starch/PVA scaffolds exhibited significant decomposition below 250°C. The inclusion of CuO NPs notably delayed the onset of thermal degradation and minimized mass loss, highlighting their contribution to improving the thermal robustness of the scaffold. Such enhancement is crucial for biomedical applications that require thermal sterilization or heat resistance [53].

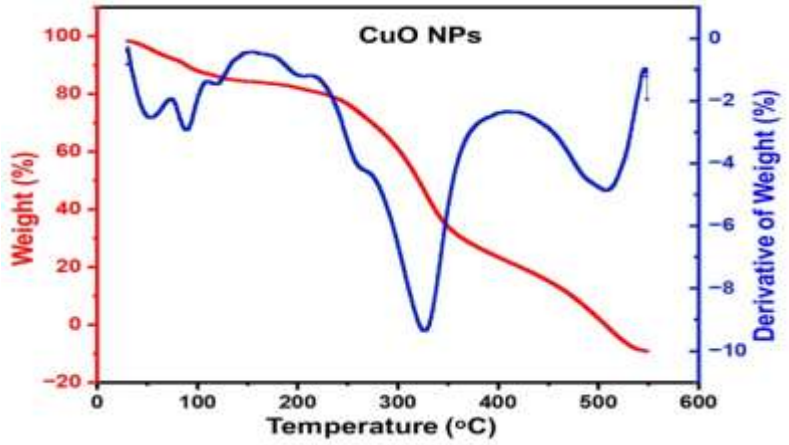

Figure 5: TGA analysis of starch/PVA electrospun nanoscaffolds

3.6. Zeta potential and particle size analysis

DLS analysis conducted at 25°C provided insights into the size and stability of the CuO NP suspension. The recorded Z-average hydrodynamic diameter was 125.6 nm (Figure 6), with a polydispersity index (PDI) of 0.475, signifying moderate size variation within the colloidal system. The particle size distribution profile (Figure 7) displayed three distinct peaks: a dominant one at 881.5 nm (84.89% intensity), a secondary at 128.3 nm (12.06%), and a minor peak at 5350 nm (3.06%), suggesting partial nanoparticle agglomeration. Zeta potential analysis, using electrophoretic light scattering, revealed a value of –10.03 mV, which falls below the ±30 mV threshold for robust colloidal stability. This suggests moderate stability, likely maintained through steric hindrance provided by phytochemical surface coatings. Supporting parameters included a conductivity of 0.1813 mS/cm, dispersant viscosity of 0.887 cP, and a dielectric constant of 78.5. The instrument's quality factor was 1.754, ensuring the validity of the measurements. Nonetheless, to enhance long-term colloidal stability for biomedical use, further surface functionalization or stabilizer incorporation may be necessary [54].

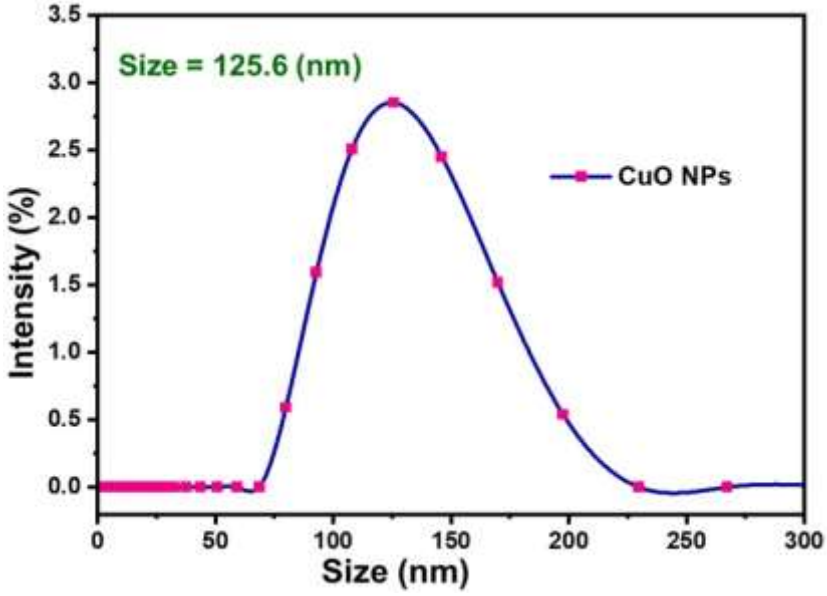

Figure 6: DLS particle size analysis of CuO NPs

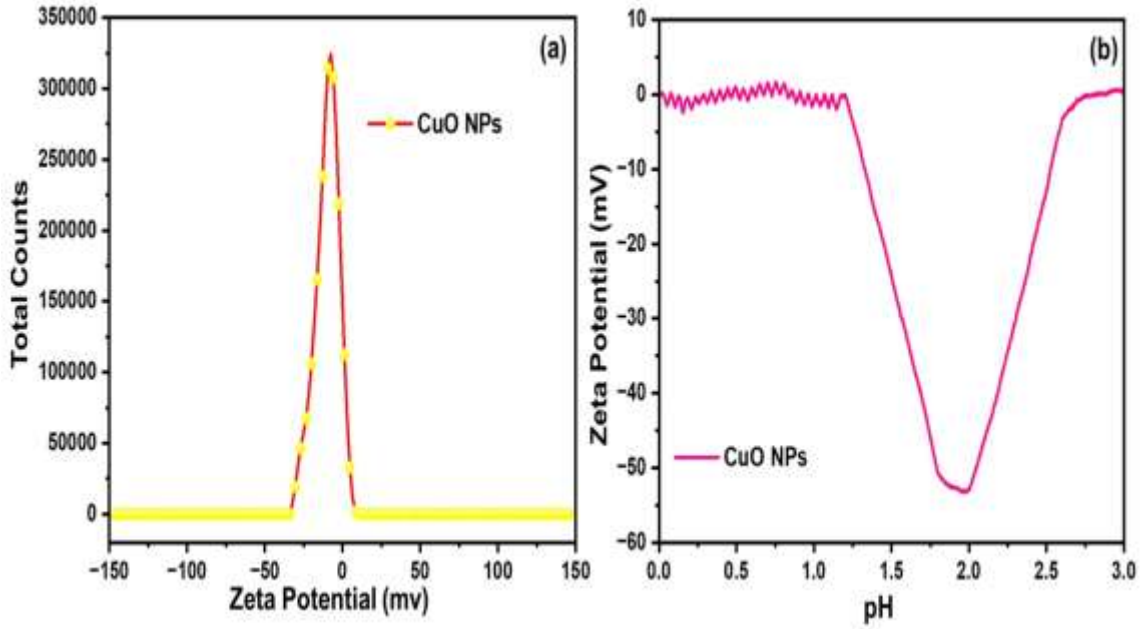

Figure 7: Zeta potential analysis of CuO NPs

3.7. Wound healing (scratch) assay

The wound healing (scratch) assay (Figure 8) demonstrated distinct migratory responses of HaCaT keratinocyte cells when treated with algal extract, CuO NPs, and starch/PVA/CuO-NPs nanoscaffolds. At the initial concentration of 6.25 µg/mL, all three test samples exhibited similar wound closure rates (26%), comparable to the untreated control. However, as the concentration increased, significant differences in efficacy emerged.

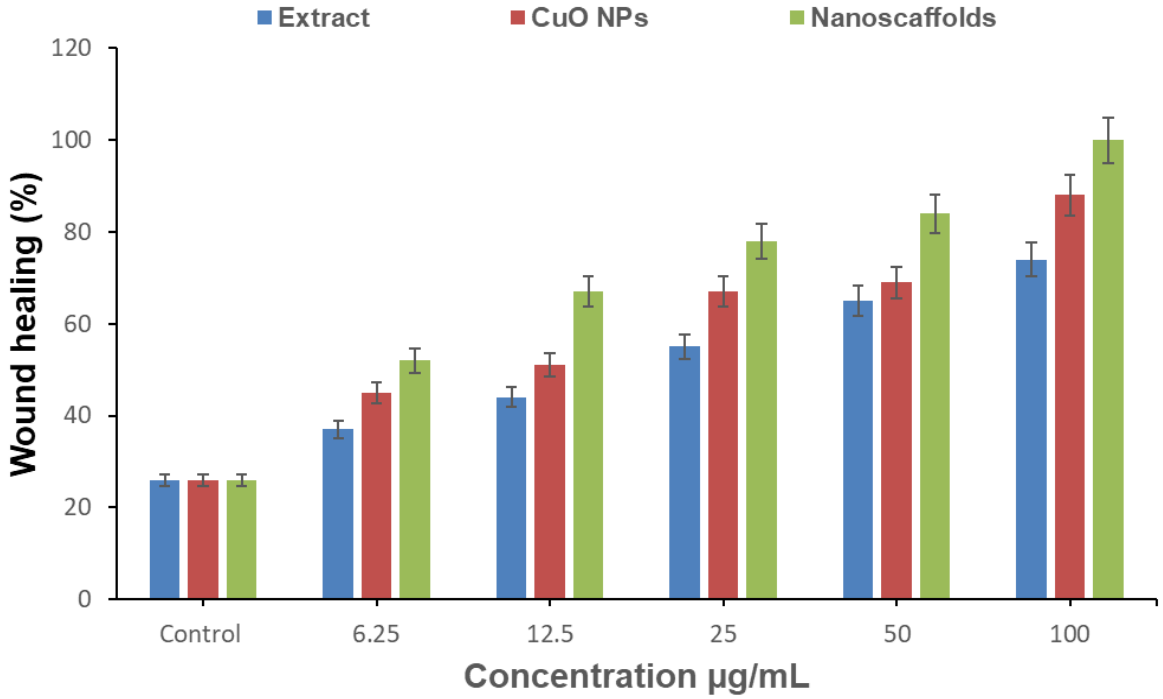

Figure 8: Wound healing potential of algal extract, CuO NPs and starch/PVA/CuO-NPs nanoscaffolds

The algal extract showed a progressive increase in wound closure, with rates rising from 37% at 12.5 µg/mL to 74% at 100 µg/mL. This suggests a concentration-dependent enhancement in cell migration, likely due to bioactive compounds in the extract promoting keratinocyte proliferation and motility. In contrast, CuO NPs exhibited a more pronounced effect, achieving 45% closure at 12.5 µg/mL and peaking at 88% at the highest concentration (100 µg/mL). The superior performance of CuO NPs may be attributed to their inherent antimicrobial and pro-regenerative properties, which could synergistically accelerate wound repair. The starch/PVA/CuO-NPs nanoscaffolds displayed the most remarkable wound healing activity, with closure rates escalating from 52% at 12.5 µg/mL to 100% at 100 µg/mL. This outstanding result highlights the scaffold's dual role as a physical support for cell adhesion and a delivery system for CuO NPs, optimizing cell migration and tissue regeneration. The nanoscaffold's biocompatible polymer matrix (starch/PVA) likely enhanced cellular interactions, while the embedded CuO NPs contributed bioactive effects, collectively maximizing wound closure efficiency [55].

All test samples promoted wound healing in a concentration-dependent manner, with the starch/PVA/CuO-NPs nanoscaffolds exhibiting the highest efficacy. These findings underscore the potential of nanoscaffolds as advanced wound dressings, combining structural and functional advantages to accelerate tissue repair.

DISCUSSION

The current study provides compelling evidence for the successful biosynthesis, characterization, and biomedical evaluation of macroalgae-derived CuO NPs incorporated into starch/PVA nanofibrous scaffolds. A comprehensive suite of analytical techniques was employed to elucidate the physicochemical properties, stability, and therapeutic potential of these biomaterials. Each analytical outcome contributes to the overall understanding of the material's functionality and highlights its applicability in wound healing [56, 57].

The UV–Visible spectroscopy analysis revealed a prominent absorption peak at 267 nm for the macroalgal extract, indicating the presence of secondary metabolites such as phenolics or other aromatic compounds. These compounds likely played a critical role in reducing copper ions during nanoparticle formation and also contributed to the stability of the synthesized CuO NPs. The emergence of a new surface plasmon resonance (SPR) band at 292 nm for CuO NPs confirms successful nanoparticle formation and a possible blue shift from traditional CuO absorption ranges due to reduced particle size or strong interaction with capping agents. The sharp absorbance and narrow band width also imply uniform particle formation with limited aggregation—a key feature for biomedical applications, where homogeneity and stability are crucial [58-61].

FTIR spectroscopy further reinforced these findings by identifying functional groups involved in nanoparticle synthesis and scaffold integration. The presence of hydroxyl, amine, and aromatic ring vibrations confirms that phytochemicals from the algal extract acted as natural stabilizers or reducing agents. The clear signals attributed to Cu–O bonding validate the formation of CuO NPs. In the starch/PVA matrix, characteristic polymeric peaks remained intact, with additional shifts and new bands (e.g., carbonyl stretching) indicating successful nanoparticle embedding and possible hydrogen bonding. Such molecular interactions not only confirm the integration of CuO within the polymer network but also suggest enhanced mechanical and chemical stability [62-65].

XRD analysis provided insight into the crystalline structure of both CuO NPs and the composite nanoscaffold. The sharp, well-defined peaks aligned with monoclinic CuO, with no signs of Cu_2O or other impurities, confirming phase purity. The narrow full width at half maximum (FWHM) values and calculated crystallite sizes between 20–50 nm are consistent with nanoscale dimensions. In the starch/PVA scaffold, the appearance of broader peaks with attenuated CuO signatures suggested successful nanoparticle encapsulation and semi-crystalline behavior. These features are desirable for wound healing applications, where controlled degradation and sustained release of bioactive agents are necessary [66, 67].

SEM analysis confirmed the morphological traits of the materials. The biosynthesized CuO NPs exhibited predominantly spherical shapes with minor agglomeration, possibly due to residual phytochemicals. The electrospun nanofibrous scaffold demonstrated a uniform, bead-free fibrous structure with embedded CuO NPs dispersed along the fiber length. The fiber diameter ranged between 150–300 nm, and high porosity was evident—an advantageous trait for promoting cell migration, nutrient exchange, and gas permeability in wound dressings. The uniform dispersion of nanoparticles without compromising the fiber structure suggests a successful fabrication strategy for producing multifunctional nanoscaffolds [68-71].

Thermal behavior, as assessed by TGA, highlighted the stability imparted by CuO NPs to the polymer matrix. The scaffold experienced a three-stage degradation pattern, with the primary degradation phase delayed to higher temperatures due to nanoparticle incorporation. Compared to native starch/PVA, which degraded more readily below 250°C, the CuO-loaded scaffold exhibited improved thermal resistance. This is critical for applications requiring thermal sterilization or high-temperature exposure during storage or clinical use [72, 73].

DLS and zeta potential analysis offered insights into the colloidal behavior of the CuO NPs. The hydrodynamic diameter was measured at 125.6 nm, with a polydispersity index of 0.475, reflecting a moderately uniform distribution. However, the presence of secondary and tertiary peaks in the size distribution graph indicates partial aggregation, which could affect long-term stability. The zeta potential of –10.03 mV implies moderate colloidal stability, attributed to steric repulsion rather than electrostatic stabilization. While sufficient for short-term applications, enhancing long-term stability may require surface functionalization with biocompatible polymers or surfactants [74].

The wound healing assay provided perhaps the most significant functional validation of the developed nanoscaffold. All test samples demonstrated dose-dependent enhancement of HaCaT cell migration, affirming their biocompatibility and bioactivity. Notably, the CuO-loaded nanoscaffold exhibited complete wound closure at the highest concentration tested (100 µg/mL), outperforming both the crude extract and isolated CuO NPs. This superior performance is likely due to the synergistic effect of the scaffold's physical structure and the embedded bioactive nanoparticles. The scaffold likely acted as a favorable substrate for cell adhesion and migration, while the CuO NPs contributed antimicrobial and regenerative properties, facilitating faster wound repair [75, 76].

Collectively, these findings underscore the potential of macroalgae-mediated green-synthesized CuO NPs embedded within starch/PVA nanofibers as an effective and multifunctional biomaterial. The integrated approach capitalizes on the bioreductive capability of algal phytochemicals, the structural advantages of electrospun nanofibers, and the antimicrobial/pro-regenerative benefits of copper-based nanomaterials. This combinatorial system presents a promising strategy for developing next-generation wound dressings that are not only biocompatible and thermally stable but also therapeutically potent. Further in vivo studies and long-term stability assessments are warranted to translate these findings into clinical applications.

CONCLUSION

This study successfully demonstrated the green synthesis, characterization, and wound healing efficacy of algal extract, CuO NPs, and starch/PVA/CuO-NPs nanoscaffolds. Spectroscopic and microscopic analyses confirmed the formation of stable, crystalline CuO NPs (20–50 nm) with bioactive phytochemical capping, while the nanoscaffold exhibited a porous, fibrous structure ideal for cell adhesion and nutrient exchange. The incorporation of CuO NPs enhanced the scaffold's thermal stability and mechanical integrity, as evidenced by TGA and XRD. In vitro wound healing assays revealed concentration-dependent cell migration, with the algal extract (74% closure) and CuO NPs (88% closure) showing significant regenerative potential. However, the starch/PVA/CuO-NPs nanoscaffold outperformed both, achieving complete wound closure (100%) at 100 µg/mL, owing to its dual role as a bioactive delivery system and structural support for keratinocyte proliferation. These results underscore the scaffold's promise as a multifunctional wound dressing, combining the antimicrobial and pro-healing properties of CuO NPs with the biocompatibility of natural polymers. Future studies should explore in vivo applications to validate its clinical potential for chronic wound management.

Ethical Declaration: Not applicable for this study.

Funding: Not available for this study.

Conflicts of Interest: The authors declare no conflicts of interest.

Data Availability Statement: The full dataset of physiochemical characterization associated with this work is published in Mendeley Data [Dataset] Physiochemical characterization of fabricated starch-based nanoscaffolds incorporated with *Pocockiella variegata* extract-mediated green synthesised copper oxide nanoparticles (DOI: 10.17632/6tddv74p8k.1).

Disclosure: The material characterization data and figures (e.g., UV, SEM, FTIR, XRD, TGA, Zeta Potential and particle sizer) presented here were generated from a common dataset and are being reused across multiple related studies on nanomaterials. All biological analyses and conclusions are original to each manuscript.

REFERENCES

1. Natarajan PM. Dental Bioinformnatics-Current Scope and Future perspectives. Research Journal of Pharmacy and Technology. 2022;15(5):2351-6.
2. Vidhyarekha U, Natarajan PM, Bhuminathan S, Sabarinathan J, Suba R, Vijayalakshmi P. Role of artificial intelligence in Oral Cancer. Advances in Public Health. 2024. 2024: 3664408.
3. Ganesan A, Kumar NG, Natarajan PM, Gauthaman J. Automated classification of elongated styloid processes using deep learning models-an artificial intelligence diagnostics. Frontiers in Oral Health. 2025; 5: 1424840.
4. Umapathy VR, Natarajan PM, Swamikannu B. Regenerative Strategies in Dentistry: Harnessing Stem Cells, Biomaterials and Bioactive Materials for Tissue Repair. Biomolecules. 2025; 15: 546.
5. Natarajan PM, Umapathy VR, Murali A, Swamikannu B. (2022). Computational Simulations of Identified marine-derived Natural Bioactive Compounds As Potential Inhibitors of Oral Cancer. Future Science OA. 2022; 8(3).
6. Ganesan A, Kumar NG, Natarajan PM. Solanum trilobatum leaf extract-derived silver nanoparticles downregulate the PI3K/AKT/mTOR signaling pathway and attenuate oral squamous cell carcinoma cell proliferation. Journal of Herbmed Pharmacology. 2024; 13(2): 300-307.
7. Perumal MKK, Renuka RR, Subbiah SK, Natarajan PM. Artificial intelligence-driven clinical decision support systems for early detection and precision therapy in oral cancer: a mini review. Frontiers in Oral Health. 2025; 6: 1592428.
8. Surendran N, Chandrasekaran G, Raju MV, Chandrasekaran MK, Ahalliya RM, Palanisamy CP, Kanniappan GV, Arcot R, Alharbi NS, Thiruvengadam M. Anti-inflammatory potential of ethanolic extract of Maranta arundinacea L.: Insights from COX-2 modulation and oxidative stress analysis. South African Journal of Botany. 2026; 195: 142-151.
9. Ponnusamy B, Rajagopal P, Palanisamy CP, Veeraraghavan VP, Jayaraman S. Mechanistic Exploration of the anticancer activity of Justicia adhatoda Plant Leaf Ethanolic Extract against Colon Cancer Cells: An in silico and in vitro Approach. Asian Pacific Journal of Cancer Prevention. 2026; 27(3): 1069-1080.
10. Pei J, Saran VS, Sivaramakrishnan R, Kanniappan GV, Pandurangan V, Jayaraman S, Dhayalan VK, Mironescu M, Mironescu ID, Palanisamy CP. Ultrasonic-assisted, Sargassum ilicifolium (brown marine macroalgae)-mediated biogenic synthesis of CuO nanoparticles incorporated in starch/PVA electrospun nanoscaffolds: In vitro safety and antioxidant efficacy assessment. Bioorganic Chemistry. 2026; 173: 109679.
11. Raj MAPA, Subramaniyam S, Kanniappan GV, Jayaraman S, Palanisamy CP. Sustainable fabrication of starch/PVA/CuO electrospun nanoscaffolds from Turbinaria ornata (marine macroalgae) extract: Physicochemical characterization and antidiabetic evaluation. Kuwait Journal of Science. 2026; 53(2): 100545.
12. Pei J, Ganesh NS, Subramaniyam S, Sivaramakrishnan R, Kanniappan GV, Jayaraman S, Palanisamy CP. Sustainable fabrication of starch/PVA/CuO electrospun nanoscaffolds from Padina tetrastromatica (Brown macroalgae) extract: Physicochemical characterization and antidiabetic assessment. Sustainable Chemistry One World. 2026; 9: 100195.
13. Sakthiraj A, Sivaramakrishnan R, Subramaniyam S, Kanniappan GV, Pandurangan V, Jayaraman S, Dhayalan VK, Mironescu M, Mironescu ID, Palanisamy CP. Chemical Physics Impact. Starch/PVA electrospun nanoscaffolds loaded with ultrasonic-assisted green-synthesis of CuO nanoparticles from marine macroalgae (Gracilaria corticata) extract: Cytotoxicity and antioxidant analysis. 2026; 12: 101018.
14. Raju M, Chandrasekaran MK, Loganathan L, Ahalliya RM, Mironescu M, Mironescu ID, Palanisamy CP, Kanniappan GV. Lipid remodeling and ferroptosis in phosphatidylcholine-mediated tumor–stroma crosstalk. Frontiers in Molecular Biosciences. 2026; 13: 1742305.

15. Kunamalla R, Panagal M, Palanisamy CP. Biogenic synthesis and fabrication of starch/PVA/CuO electrospun nanoscaffolds from Sargassum ilicifolium (brown marine macroalgae) extract for anticancer activity on HT-29 and MCF-7 cancer cells. Biocatalysis and Agricultural Biotechnology. 2026; 72: 103923.
16. Rajendran MS, Jayaraman S, Khan JM, Jasmine S, Prabhakaran RK, Raju MV, Chandrasekaran MK, Ahalliya RM, Kannappan P, Palanisamy CP, Kanniappan GV. Investigating the colon toxicity and carcinogenic role of monosodium glutamate compared with Dimethylhydrazine in male Wistar rats: Exploring the link to childhood colon cancer risk. Journal of King Saud University - Science. 2024; 36(11): 103507.
17. Kumarasamy RV, Natarajan PM, Umapathy VR, Roy JR, Rab SO, Saeed M, Panagal M, Mironescu M, Srinivasan GP, Palanisamy CP. Clinical Applications and Therapeutic Potentials of Advanced Nanoparticles: A Comprehensive Review on Completed Human Clinical Trials. Frontiers in Nanotechnology. 2024; 6:1479993.
18. Jin W, Pei JJ, Roy JR, Jayaraman S, Ahalliya RM, Kanniappan GV, Mironescu M, Palanisamy CP. Comprehensive review on single-cell RNA sequencing: A new frontier in Alzheimer's disease research. Ageing Research Reviews. 2024; 274: 102454.
19. Pei J, Palanisamy CP, Jayaraman S, Natarajan PM, Umapathy VR, Roy JR, Panagal M, Jayaraman S. Curcumin-loaded polymeric nanomaterials as a novel therapeutic strategy for Alzheimer's disease: A comprehensive review. Ageing Research Reviews. 2024; 99: 102393.
20. Pei J, Govindaraj H, Sivaramakrishnan R, Kanniappan GV, Pandurangan V, Dhayalan VK, Mironescu M, Mironescu ID, Jayaraman S, Palanisamy PC. Sustainable fabrication of biopolymer-based (starch/PVA) nanoscaffolds loaded with green-synthesized CuO nanoparticles from Sargassum wightii (marine macroalgae): Cytocompatibility and antioxidant activity. Biomaterials Advances. 2026; 182: 214660.
21. Pei J, Perumal NC, Meng P, Long Q, Palanisamy CP. Extracellular vesicle-based biosensors for Alzheimer's disease: A new frontier in precision diagnostics. Ageing Research Reviews. 2026; 113: 102904.
22. Shree P, Sivaramakrishnan R, Kanniappan GV, Pandurangan V, Jayaraman S, Dhayalan VK, Mironescu M, Mironescu ID, Palanisamy CP. Antioxidant and biocompatible CuO-starch/PVA nanoscaffolds via ultrasonic green synthesis using Turbinaria conoides (brown marine macroalgae). Medicine in Drug Discovery. 2025; 28: 100238.
23. Gong J, Lin J, Guan T, Pei J, Palanisamy CP, El-AtyFrom AMA. selenium tolerance to nanoplastic antagonism: Comprehensive characterization of L. casei SNUT1 and its extracellular vesicle–nanoselenium complex. Food Bioscience. 2025; 74: 107749.
24. Poochi SP, Sundarraj R, Raju MV, Chandrasekaran MK, Ahalliya RM, Palanisamy CP, Kanniappan GV, Kondapavuluri BK, Thiruvengadam M. Harnessing Nature: Computational and Experimental Insights Into Ipomoea obscura Metabolites for Bladder Cancer Therapy. Chemistry and Biodiversity. 2025; 0: e00909.
25. Dugganaboyana GK, Kannankumar MKG, Shivaramakrishna S, Raju MV, Chandrasekaran MK, Ahalliya RM, Panneerselvam N, Palanisamy CP, Kanniappan GV. Phytochemical insights, antioxidant activity and therapeutic potential of Cassia senna against prostate cancer in Wistar albino rats. Discover Applied Sciences. 2025; 7:1206.
26. Natarajan SR, Krishnamoorthy R, Alshuniaber MA, Gatasheh MK, Rajagopal P, Veeraraghavan VP, Palanisamy CP, Jayaraman S. KDM1A Facilitates Oncogenic Potential in Colorectal Cancer Progression Through the Activation of AXIN/GSK3β/β-Catenin Signaling Pathways: Evidence From Integrated Transcriptomics and In Vitro Studies. The Journal of Gene Medicine. 2025; 27(11): e70053.
27. Guan T, Gong J, Lin J, Palanisamy CP, Jinjin Pei J, El-Aty AMA. Machine learning-driven multimodal optimization of selenium biotransformation and flavor profiling in fermented apple–Yacon functional beverages. Innovative Food Science & Emerging Technologies. 2025; 105: 104198.
28. Ramesh E, Ganesan A, Lakshmi KC, Natarajan PM. Artificial intelligence-based diagnosis of oral leukoplakia using deep convolutional neural networks Xception and MobileNet-v2. Frontiers in Oral Health. 2025; 6: 1414524.
29. Natarajan PM. Computational Studies on Recent Congeners of Fluoroquinolones and Nitroimidazoles for Their Use in Periodontal Therapy. Journal of Pharmacy and Bioallied Sciences. 2024; 16(5): S4731-S4740.
30. Ganesan A, Kumar NG, Natarajan PM. Anticancer activity of silver nanoparticles synthesized from aqueous leaf extract of Solanum trilobatum (Purple fruit pea eggplant) on human oral cancer cells. Journal of Herbmed Pharmacololgy. 2024; 13(2): 260-268.
31. Umapathy V, Dhanavel A, Kesavan R, Natarajan PM, Bhuminathan S, Vijayalakshmi P. Anticancer Potential of the Principal Constituent of Piper nigrum, Piperine: A Comprehensive Review. Cureus. 2024; 16(2): e54425.
32. Natarajan PM, Bhuminathan S, Rajan R, Bindu K, Loganathan K, Veerakumar R. The Crucial Role of Smoking Cessation in Preventing Oral Cancer. Journal of Pharmacy and Bioallied Sciences. 2024; 16(5): S4245-S4247.
33. Umapathy VR, Swamikannu B, Natarajan PM, Devi R, Nandini MS, Vimalarani, Vijayalakshmi P. In Silico Molecular Docking of Ocimum sanctum Phytochemicals: Targeting Key Biomarkers in Oral Cancer. Journal of Pharmacy and Bioallied Sciences. 2024; 16(5): S4792-S4799.
34. Natarajan PM, Umapathy VR. Role of transcriptomics in the study of oral cancer. Frontiers in Oral Health. 2025; 6:1524364.
35. Swamikannu B, Umapathy VR, Natarajan PM, Nandini MS, Stylin AGSQ, Vimalarani V, Rajinikanth S. Unlocking the Therapeutic Benefits of Artemisia Annua: A Comprehensive Overview of its Medicinal Properties. Journal of Pharmacy and Bioallied Sciences. 2024; 16(5): S4248-S4253.
36. Natarajan SR, Krishnamoorthy R, Alshuniaber MA, Alsulami TS, Gatasheh MK, Rajagopal P, Palanisamy CP, Govindan R, Veeraraghavan VP, Jayaraman S. ABCE1 facilitates tumour progression via aerobic glycolysis and inhibits cell death in human colorectal cancer cells through the p53 signalling pathway. Scientific Reports. 2025; 15: 24674.
37. Huang Y, Guo H, Liu Y, Jin W, Palanisamy CP, Pei J, Oz F, El-Aty AMA. Effects of Natural Polysaccharides on the Gut Microbiota Related to Human Metabolic Health. Molecular Nutrition & Food Research. 2025; 69:e202400792.

38. Poornima K, Meenakshi K.C, Manikandan V.R, Shankari G, Prabhu D, Rathi M.A, Palanisamy CP, Balaji R, Gopalakrishnan V.K. Exploring the anticancer potential of Jerantinine A from Tabernaemontana coronaria against prostate, breast, and ovarian cancers: A computational approach. Journal of Complementary and Integrative Medicine, 2025 22(2): 363–372.
39. Guo H, Liu Y, Wan T, Song D, Palanisamy CP, Geng J, Pei J, Özmen S, El-Aty AMA. Toward personalized cancer management: Role of precision nutrition–diet interventions. Journal of Functional Foods. 2024; 123: 106584.
40. Natarajan SR, Krishnamoorthy R, Alshuniaber MA, Al-Anazi KM, Farah MA, Rajagopal P, Palanisamy CP, Veeraraghavan VP, Jayaraman S. Identification of FOXM1 as a novel protein biomarker and therapeutic target for colorectal cancer progression: Evidence from immune infiltration and bioinformatic analyses. International Journal of Biological Macromolecules. 282 (Part 4): 137201.
41. Pei J, Palanisamy CP, Jayaraman S, Natarajan PM, Umapathy VR, Roy JR, Thalamati D, Ahalliya RM, Kanniappan GV*, Mironescu M. A comprehensive review on starch-based Sustainable Edible Films Loaded with Bioactive Components for Food Packaging. International Journal of Biological macromolecules. 2024; 274 (Part-1): 133332.
42. Palanisamy CP, poompradub S, Sansanaphongpricha K, Subramani K, Sonsudin F. Increased expression levels of PDGF and VEGF magnify the wound healing potential facilitated by biogenic synthesis of silver nanoparticles. Nano-Structures & Nano-Objects. 2024; 39: 101236.
43. Pei J, Palanisamy CP, Jayaraman S, Natarajan PM, Umapathy VR, Roy JR, Thalamati D, Ahalliya RM, Kanniappan GV, Mironescu M. Proteomics Profiling of Extracellular Vesicle for Identification of Potential Biomarkers in Alzheimer's Disease: A Comprehensive Review. Ageing Research Reviews. 2024; 99: 102359.
44. Xi J, Wang T, Xian P, Liu X, Du M, Yang H, Palanisamy CP, Lin W, Long Q. Proteomic insights uncover enhanced neurotherapeutic potential in conditioned mesenchymal stem cell-derived extracellular vesicles. Extracellular Vesicle. 2024; 3: 100037.
45. Palanisamy CP, Poompradub S, Sansanaphongpricha K, Jayaraman S, Subramani K. Faridah Sonsudin gGreen synthesis of Nigella sativa-mediated silver nanoparticles for enhanced antibacterial activity and wound healing: Mechanistic insights and biomedical applications. Environmental Nanotechnology, Monitoring & Management. 2025; 24: 101085.
46. Surendran N, Raju MV, Chandrasekaran MK, Ahalliya RM, Palanisamy CP, Chandrasekaran G, Kanniappan GV. Physicochemical characterization of starch from Maranta arundinacea L.(arrowroot) rhizomes and its inhibition of COX-2: In vivo validation. Bioactive Carbohydrates and Dietary Fibre. 2025; 33: 100465.
47. Pei J, Senthilkumar MV, Hessini K, Subramaniyam S, Sivaramakrishnan R, Kanniappan GV, Jayaraman S, Palanisamy CP. Green fabrication of starch/PVA/CuO nanoscaffolds using marine macroalgae extract for enhanced anti-inflammatory activity. Sustainable Chemistry and Pharmacy. 2026; 51: 102397.
48. Balasubramanian V, Loganathan L, Muthuswamy K, Viswanathan TM, Raju MV, Chandrasekaran MK, Ahalliya RM, Poorasamy J, Palanisamy CP, Dominic S, Kanniappan GV. Anticancer therapeutic efficacy of PEGylated β-galactosidase from Aspergillus terreus in DMBA-induced breast cancer: Toxicological, molecular and histopathological evaluation in Wistar rats. International Journal of Biological Macromolecules. 2026; 360: 151856.
49. Jayaraman S, Eswaran A, Rajagopal P, Palanisamy CP, Veerakumar P, Veeraraghavan VP, Sirasanagandla SR. Neuroendocrine-associated epigenetic factors in cellular senescence: mechanisms and therapeutic implications. Biogerontology. 2026; 27(2): 64.
50. Kannappan P, Chandrasekaran MK, Raju MV, Gopalakrishnan S, Dhamodharan P, Ahalliya RM, Palanisamy CP, Raju B, Kanniappan GV. Exploring the anticancer potential of Jerantinine A from Tabernaemontana coronaria against prostate, breast, and ovarian cancers: a computational approach. Journal of Complementary and Integrative Medicine. 2025; 22(02): 363-372.
51. Yadalam PK, Arumuganainar D, Natarajan PM, Ardila CM. Artificial intelligence-powered prediction of AIM-2 inflammasome sequences using transformers and graph attention networks in periodontal inflammation. Scientific Reports. 2025; 15: 8733.
52. Yadalam PK, Chatterjee S, Natarajan PM, Ardila CM. Comparison of light gradient boosting and logistic regression for interactomic hub genes in Porphyromonas gingivalis and Fusobacterium nucleatum-induced periodontitis with Alzheimer's disease. Frontiers in Oral Health. 2025; 6:1463458.
53. Natarajan PM, Bhuminathan S, Leela B, Bindu K, Loganathan K, Ramachandran V. Smoking and its Role in Oral Cancer. Journal of Pharmacy and Bioallied Sciences 16(5): S4242-S4244.
54. Yadalam PK, Natarajan PM, Ardila CM. Variational graph autoencoder for reconstructed transcriptomic data associated with NLRP3 mediated pyroptosis in periodontitis. Scientific Reports. 2025; 15: 1962.
55. Natarajan PM, Swamikannu B, Sivaraman NM, Stylin AGSQ. Prevention of Oral Cancer: A Comprehensive Guide. Journal of Pharmacy and Bioallied Sciences. 2024; 16(5): S4239-S4241.
56. Pei J, Kumarasamy RV, Jayaraman S, Kanniappan GV, Long Q, Palanisamy CP. Quercetin-functionalized nanomaterials: Innovative therapeutic avenues for Alzheimer's disease management. Ageing Research Reviews. 2025; 104: 102665.
57. Jayaraman S, Prasad M, Natarajan SR, Krishnamoorthy R, Alshuniaber MA, Gatasheh MK, Veeraraghavan VP, Rajagopal P, Palanisamy CP. Molecular mechanisms underlying the effects of beta-sitosterol on TGF-β1/Nrf2/SIRT1/p53-mediated signaling in the kidney of a high-fat diet and sucrose-induced type-2 diabetic rat. Chemico-Biological Interactions. 2025; 411: 111443.
58. Huang Y, Guo H, Liu Y, Jin W, Palanisamy CP, Pei J, Oz F, El-Aty AMA. Effects of Natural Polysaccharides on the Gut Microbiota Related to Human Metabolic Health. Molecular Nutrition & Food Research. 2025; e202400792.

59. Prabhakaran P, Palanisamy CP, Shanmugam A, Damodharan P, Swaminathan H, Devaraj D, Ahalliya RM, Kanniappan GV. Isolation, structural characterization, and molecular docking studies on the bioactive compound from n-Hexane extract of Emilia sonchifolia (L.) DC against the pancreatic cancer target Aurora 2 Kinase. Journal of Complementary and Integrative Medicine. 2024; 22(1): 0290.
60. Jiang H, Kumarasamy RV, Pei J, Raju K, Kanniappan GV, Palanisamy CP. Integrating engineered nanomaterials with extracellular vesicles: Advancing targeted drug delivery and biomedical applications. Frontiers in Nanotechnology. 2024; 6: 1513683.
61. Pei J, Natarajan PM, Umapathy VR, Swamikannu B, Sivaraman NM, Krishnasamy L, Palanisamy CP. Advancements in the synthesis and functionalization of zinc oxide-based nanomaterials for enhanced oral cancer therapy. Molecules. 2024; 29(11): 2706.
62. Gatasheh MK, Natarajan SR, Krishnamoorthy R, Alsulami TS, Rajagopal P, Palanisamy CP, Veeraraghavan VP, Jayaraman S. Molecular analysis to identify novel potential biomarkers as drug targets in colorectal cancer therapy: an integrated bioinformatics analysis. Molecular and Cellular Oncology. 2024; 11(1): 2326699.
63. Pei J, Yan Y, Jayaraman S, Rajagopal P, Natarajan PM, Umapathy VR, Gopathy S, Roy JR, Sadagopan CS, Thalamati D, Palanisamy CP, Mironescu M. A review on advancements in the application of starch-based nanomaterials in biomedicine: Precision drug delivery and cancer therapy. International Journal of Biological Macromolecules. 2024; 130746.
64. Pei JJ, Yan Y, Palanisamy CP, Jayaraman S, Natarajan PM, Umapathy VR, Gopathy S, Roy JR, Sadagopan JC, Thalamati D, Mironescu M. Materials-based drug delivery approaches: Recent advances and future perspectives. Green Processing and Synthesis. 2024; 13: 20230094.
65. Panneerselvam S, Viswaja K, Deepa E, Prathiba S, Rebecca FS, Nivedha RP, Rajagopal P, Veeraraghavan VP, Sridevi G, Palanisamy CP, Jayaraman S. Hypoglycemic Potential of Acalypha indica in Streptozotocin-Induced Type 2 Diabetic Rats. International Journal of Drug Delivery Technology. 2026; 16(26s):1038-1047.
66. Panneerselvam S, Viswaja K, Prathiba S, Rebecca FS, Nivedha RP, Rajagopal P, Fathima SJH, Veeraraghavan VP, Sridevi G, Palanisamy CP, Jayaraman S. Acalypha Indica Attenuates Insulin Resistance in STZ-Induced Type 2 Diabetic Male Rats: Mechanistic Study. International Journal of Drug Delivery Technology. 2026; 16(26s):1027-1037.
67. Manju NE, Natarajan A, Rebecca FS, Nivedha RP, Hemalatha R, Rajagopal P, Murali R, Veeraraghavan VP, Sridevi G, Palanisamy CP, Jayaraman S. Effect of Seendhil polyherbal formulation in attenuating type-2 diabetes in STZ-induced experimental rats. International Journal of Drug Delivery Technology. 2026; 16(26s):981-989.
68. Manju NE, Natarajan A, Rebecca FS, Nivedha RP, Hemalatha R, Rajagopal P, Murali R, Veeraraghavan VP, Sridevi G, Palanisamy CP, Jayaraman S. Molecular mechanism to identify the effects of Seendhil polyherbal preparation on IRS-1/AKT/GLUT4/NRF2-KEAP-1 mediated signaling in SFZ-induced type-2 diabetic adult male rats. International Journal of Drug Delivery Technology. 2026;16(26s):972-980.
69. Palanisamy CP, Poompradub S, Sansanaphongpricha K, Jayaraman S, Subramani K, Sonsudin F. Biosynthesis of silver nanoparticles (AgNPs) using ethanolic extract of Nigella sativa (L.) seeds promotes wound healing via PDGF and VEGF signalling pathways activation. Biocatalysis and Agricultural Biotechnology. 2023; 54: 102970.
70. Palanisamy CP, Pei JJ, Phaniendra A, Venkata AAN, Jayaraman S, Veeraragahavan VP, Sridevi G, Roy JR, Janaki CS, Thalamati D, Mironescu M, Luo Q, Chai Y, Long Q. New Strategy of Neurodegenerative Disease Treatment with Extracellular Vesicles (EVs) Derived from Mesenchymal Stem Cells (MSCs). Theranostics. 2023; 13(12):4138-4165.
71. Potekaev NN, Borzykh OB, Medvedev GV, Pushkin DV, Petrova MM, Petrov AV, et al. The role of extracellular matrix in skin wound healing. Journal of Clinical Medicine. 2021;10(24):5947.
72. Mirhaj M, Labbaf S, Tavakoli M, Seifalian AM. Emerging treatment strategies in wound care. International Wound Journal. 2022;19(7):1934-54.
73. Graves N, Phillips C, Harding K. A narrative review of the epidemiology and economics of chronic wounds. British Journal of Dermatology. 2022;187(2):141-8.
74. Rani Raju N, Silina E, Stupin V, Manturova N, Chidambaram SB, Achar RR. Multifunctional and smart wound dressings—a review on recent research advancements in skin regenerative medicine. Pharmaceutics. 2022;14(8):1574.
75. Deng X, Gould M, Ali MA. A review of current advancements for wound healing: Biomaterial applications and medical devices. Journal of Biomedical Materials Research Part B: Applied Biomaterials. 2022;110(11):2542-73.
76. Blanco-Fernandez B, Castano O, Mateos-Timoneda MÁ, Engel E, Pérez-Amodio S. Nanotechnology approaches in chronic wound healing. Advances in wound care. 2021;10(5):234-56